Original article

MOLECULAR METABOLISM

High-calorie diet exacerbates prostate neoplasia in mice with haploinsufficiency of *Pten* tumor suppressor gene

Jehnan Liu [1,2,6], Sadeesh K. Ramakrishnan [1,2,6], Saja S. Khuder [1,2,6], Meenakshi K. Kaw [1,2,6], Harrison T. Muturi [1,2], Sumona Ghosh Lester [1,2], Sang Jun Lee [1,2], Larisa V. Fedorova [3], Andrea J. Kim [1,2], Iman E. Mohamed [3], Cara Gatto-Weis [4], Kathryn M. Eisenmann [5], Philip B. Conran [4], Sonia M. Najjar [1,2,*]

ABSTRACT

Objective: Association between prostate cancer and obesity remains controversial. Allelic deletions of *PTEN*, a tumor suppressor gene, are common in prostate cancer in men. Monoallelic *Pten* deletion in mice causes low prostatic intraepithelial neoplasia (mPIN). This study tested the effect of a hypercaloric diet on prostate cancer in $Pten^{+/-}$ mice.

Methods: 1-month old mice were fed a high-calorie diet deriving 45% calories from fat for 3 and 6 months before prostate was analyzed histologically and biochemically for mPIN progression. Because $Pten^{+/-}$ mice are protected against diet-induced insulin resistance, we tested the role of insulin on cell growth in RWPE-1 normal human prostatic epithelial cells with siRNA knockdown of PTEN.

Results: In addition to activating PI3 kinase/Akt and Ras/MAPkinase pathways, high-calorie diet causes neoplastic progression, angiogenesis, inflammation and epithelial—mesenchymal transition. It also elevates the expression of fatty acid synthase (FAS), a lipogenic gene commonly elevated in progressive cancer. SiRNA-mediated downregulation of PTEN demonstrates increased cell growth and motility, and soft agar clonicity in addition to elevation in FAS in response to insulin in RWPE-1 normal human prostatic cells. Downregulating FAS in addition to PTEN, blunted the proliferative effect of insulin (and IL-6) in RWPE-1 cells.

Conclusion: High-calorie diet promotes prostate cancer progression in the genetically susceptible *Pten* haploinsufficient mouse while preserving insulin sensitivity. This appears to be partly due to increased inflammatory response to high-caloric intake in addition to increased ability of insulin to promote lipogenesis.

Keywords PTEN tumor suppression; Hyperinsulinemia; Fatty acid synthase; Neoplasia; Prostate cancer

1. INTRODUCTION

Several prospective studies reveal an association between obesity and increased incidence and mortality of a variety of cancers [1]. However, the association between obesity and prostate cancer remains controversial. While some studies show a modest increase in the risk of high grade prostate cancer with obesity [2], others suggest no significant association [3]. Furthermore, recent meta-analysis studies relate prostate cancer to visceral obesity (higher waist circumference) more than other components of metabolic syndrome, such as dyslipidemia [4].

Prostate cancer is the second most common cause of death in males in industrialized countries that also suffer from an epidemic rise in visceral obesity. Emerging evidence supports the view that hypercaloric diet increases early-onset of prostate cancer and promotes its progression to a metastatic state [5]. Visceral obesity is associated with hyperinsulinemia commonly resulting from elevated insulin secretion as a compensatory response to peripheral insulin resistance. Enhanced insulin secretion is associated with increased risk and mortality from high grade prostate cancer [6]. Although not fully investigated, several mechanisms could be implicated in the molecular processes linking hyperinsulinemia to prostate cancer progression. These include: (i) increased insulin mitogenesis [6]; (ii) reduced apoptosis via Akt and the mammalian target of rapamycin pathways [7]; and (iii) increased transcription of fatty acid synthase (FAS), a key lipogenic enzyme in *de novo* synthesis of fatty acids that provide

[1]Center for Diabetes and Endocrine Research, The University of Toledo College of Medicine and Life Sciences, Toledo, OH, 43614, USA [2]Department of Physiology and Pharmacology, The University of Toledo College of Medicine and Life Sciences, Toledo, OH, 43614, USA [3]Department of Medicine, The University of Toledo College of Medicine and Life Sciences, Toledo, OH, 43614, USA [4]Department of Pathology, The University of Toledo College of Medicine and Life Sciences, Toledo, OH, 43614, USA [5]Department of Biochemistry and Cancer Biology, The University of Toledo College of Medicine and Life Sciences, Toledo, OH, 43614, USA

[6] Jehnan Liu, Sadeesh K. Ramakrishnan, Saja S. Khuder and Meenakshi K. Kaw contributed equally to the work.

*Corresponding author. Health Science Campus, 3000 Arlington Avenue, Mail Stop 1009, Toledo, OH, 43614, USA. Tel.: +1 (419) 383 4059; fax: +1 (419) 383 2871. E-mail: sonia.najjar@utoledo.edu (S.M. Najjar).

Received December 16, 2014 • Revision received December 22, 2014 • Accepted December 23, 2014 • Available online 2 January 2015

http://dx.doi.org/10.1016/j.molmet.2014.12.011

Abbreviations

CD31	cluster of differentiation 31
CEACAM1	carcinoembryonic antigen-related cell adhesion molecule
E-Cadherin	epithelial cadherin
EMT	epithelial mesenchymal transition
FAS	fatty acid synthase
FFA	free fatty acids
FoxP3	forkhead box protein P3
GAPDH	glyceraldehyde 3-phosphate dehydrogenase
HC	high-calorie fat-enriched diet
HIF-1α	hypoxia inducible factor-1α
IHC	immunohistochemistry
KLK2	kallikrein 2
MAPK	mitogen-activated protein kinase
MCP1	monocyte chemoattractant protein 1
MTT	3-(4,5-dimethylthiazol-2-yl)-2,5-diphenyltetrazolium bromide
mPIN	mouse intraepithelial neoplasia
N-Cadherin	neural cadherin
PCNA	proliferating cell nuclear antigen
PI3K	phosphoinositide 3-kinase
PPAR	peroxisome proliferator-activated receptor
Pten	phosphatase and tensin homolog
Pten$^{+/+}$	wild-type mice
Pten$^{+/-}$	mice with global monoallelic deletion of *Pten*
RWPE-1	normal human prostatic epithelial cells
SOX9	(sex determining region Y)-box9
SREBP	sterol regulatory element binding protein
TNFα	tumor necrosis factor alpha
siRNA	small interfering ribonucleic acid
VEGF	vascular endothelial growth factor
VEGFR	vascular endothelial growth factor receptor

energy to the rapidly proliferating cancer cells [8]. In addition to hyperinsulinemia, visceral obesity is often associated with hypercholesterolemia that plays an important role in prostate pathology, in particular benign prostate disease [9].

The tumor suppressor Phosphatase and Tensin Homolog (PTEN) targets phosphatidylinositol 3-kinase (PI3K/Akt) to act as its primary downregulator [10]. It plays a critical role in cell apoptosis and tumor suppression, not only through the PI3K/Akt pathway, but also through other independent mechanisms [11,12]. *PTEN* mutations have been identified in several sporadic tumors as well as in patients with predisposition to cancers such as Cowden disease [13]. In prostate cancer, allelic deletions of *PTEN* are more common than genetic mutations and monoallelic deletions are detected in localized prostate cancer while complete loss of *PTEN* gene occurs in metastatic, androgen-independent tumor [14,15]. In mice, global monoallelic deletion of *Pten* gene causes prostatic intraepithelial neoplasia (mPIN) that does not progress to invasive carcinoma [16]. To examine whether dietary factors promote progression of prostate cancer, *Pten* haploinsufficient male mice (*Pten*$^{+/-}$) and their wild-type counterparts (*Pten*$^{+/+}$) were fed a high-calorie fat-enriched (HC) diet for a prolonged period of time prior to evaluating the penetrance and progression of prostate neoplasia. The data indicate a synergestic effect of high-calorie diet on *Pten* haploinsufficiency in prostate cancer progression.

2. RESULTS

2.1. Metabolic effect of high-calorie diet

Consistent with insulin sensitivity [17], and protection against diet-induced insulin resistance in *Pten*$^{+/-}$ mutants [18], HC does not cause glucose intolerance (Figure 1) or lipolysis (increased fasting plasma NEFA level) (Table 1) in *Pten*$^{+/-}$ as it does in their wild-type counterparts. HC also induces insulin release (C-peptide) and plasma insulin levels only slightly, as opposed to *Pten*$^{+/+}$ mice where it exerts a stronger insulin-inducing effect (Table 1). Together, the data show preserved insulin sensitivity in *Pten*$^{+/-}$ mice despite prolonged high-calorie intake, as opposed to wild-types that develop diet-induced insulin resistance. In contrast, HC induces a comparable body weight gain (Figure S1 and Table 1) and an increase in fasting plasma cholesterol and triglycerides in both groups of mice (Table 1). As expected from increased lipid production in liver [19], and redistribution to white adipose tissue, HC also induces visceral adiposity to the same extent in mutants as in wild-types.

2.2. High-calorie diet exacerbates the neoplastic phenotype in *Pten*$^{+/-}$ prostate

Global monoallelic deletion of *Pten* causes preneoplasia in prostate [20]. To investigate whether HC feeding causes progression of neoplasia, one-month old male *Pten*$^{+/-}$ and their *Pten*$^{+/+}$ littermate controls were fed either RD or HC for 3 or 6 months prior to performing histological analysis of mPIN on the ventral and dorsolateral lobes of prostate. For simplicity, H&E sections representing the most progressive mPIN from each group of 7-month old mice are included in Figure 2A. Microscopic examination of prostates from RD- and HC-fed *Pten*$^{+/+}$ mice shows a thin fibromuscular stromal layer surrounding individual glands and a normal continuous lining of the epithelium with basal nuclear polarity of mPIN 0-1 (upper panels, hollow red arrow). Additionally, *Pten*$^{+/+}$ mice exhibit features of mPIN 1-2 where glands have flatter luminal edges with occasional crowding, infolding and tufting of epithelium (hollow black arrow). In contrast, RD-fed *Pten*$^{+/-}$ haploinsufficient mice exhibit predominantly mPIN 3 with extensive gland-in-gland proliferation inside the lumen (lower left panel, red arrow) and hyperchromatic nuclei with atypia (black arrow). HC-fed *Pten*$^{+/-}$ predominantly develop mPIN 4 with carcinoma *in situ* and more diffuse stromal invasion (lower right panel, black arrowhead).

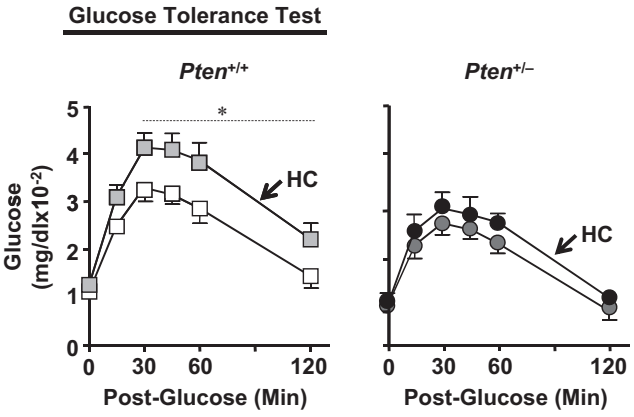

Figure 1: Metabolic effect of high-calorie diet. (A) One-month old wild-type *Pten*$^{+/+}$ (squares) and Pten$^{+/-}$ null mice (circles) were fed either regular chow (RD) or a high-calorie diet (HC) for 6 months before they were challenged with an ip injection of glucose (1.5 g/kg BW) to assess blood glucose levels at 0–120 min post-injection. *$p < 0.05$ HC vs RD per each mouse group (n > 6/feeding group).

Table 1 — Plasma biochemistry.

	Pten$^{+/+}$		*Pten*$^{+/-}$	
	RD	HC	RD	HC
Body weight (g)	29. ± 1.2	43. ± .67*	29. ± 1.3	48. ± 1.6*
Visceral obesity (%)	2.0 ± 0.1	6.3 ± 0.3*	1.7 ± 0.1	5.4 ± 0.3*
Insulin (pM)	52. ± 5.0	94. ± 3.5*	44. ± 3.2	62. ± 5.1*†
C-Peptide (pM)	719 ± 173	1324 ± 132*	652 ± 159	768 ± 111†
Glucose (mg/dl)	134. ± 9.00	147. ± 7.03*	137. ± 11.0	131. ± 13.0†
NEFA (mEq/l)	.60 ± .04	.84 ± .06*	.60 ± .21	.75 ± .07
Triglycerides (mg/dl)	47 ± 4.5	66. ± 5.0*	53 ± 3.6	81. ± 8.4*
Cholesterol (μg/μl)	93.3 ± 4.60	200. ± 17.1*	91.0 ± 2.27	220. ± 31.1*
Testosterone (pg/ml)	.27 ± .08	.11 ± .02	.24 ± .08	.21 ± .07

Mice were fed HC for 6 months and their fasting plasma biochemistry was determined together with visceral obesity and body weight. Data are expressed as mean ± SEM (n = 8–14 mice/group). *$p < 0.0125$ vs RD per mouse group and $^{\dagger}p < 0.0125$ vs same feeding regimen in *Pten*$^{+/+}$.

Moreover, some *Pten*$^{+/-}$ mice fed HC for 6 months show invasion of the basement membrane surrounding the gland with necrotic debris and inflammatory cells at the site of invasion (hollow arrowhead).

As Table 2 reveals, 93% of 4-month old *Pten*$^{+/+}$ wild-type mice exhibit mPIN 2. While the majority of age-matched *Pten*$^{+/-}$ (58%) also exhibit mPIN 2, they also develop mPIN 3 at a penetrance of 37%, 10-fold higher than wild-type animals (4%). *Pten*$^{+/-}$ mice on RD develop a more progressive neoplastic phenotype with age, as evidenced by a 2-fold increase in the penetrance of mPIN 3 in 7 vs 4-month old mice (73% vs 37%) and the development of mPIN 4 at 13% penetrance beginning at 7 months of age.

HC feeding exacerbates the phenotype of *Pten*$^{+/-}$ mice, as demonstrated by the initiation of mPIN 4 in 12% of mice fed HC for 3 months and invasive carcinoma in 21% of mice fed HC for 6 months (Table 2).

This HC effect is relatively milder in wild-type mice where it only causes mPIN 3 and mPIN 4 progression at 29% and 4% penetrance, respectively, after 3 months, and only increases penetrance of mPIN 2 (71% vs 56%) without provoking an increase in the penetrance of mPIN 3 after 6 months (14% vs 15%). This could be related to age-related factors that limits the neoplastic effect of HC in wild-type, but not *Pten*$^{+/-}$ mice. Together, the data demonstrate that HC diet exacerbates the neoplastic phenotype in the genetically predisposed *Pten*$^{+/-}$ mice, in a linear relationship with the duration of feeding period.

2.3. High-calorie intake elevates androgen receptor expression in *Pten*$^{+/-}$ prostate

Consistent with elevated androgen receptor (AR) content during progression of prostate cancer, *Pten* haploinsufficiency causes a 1.5-fold increase in the mRNA level of AR (Figure 2B). HC intake further induces AR mRNA by 2-fold in *Pten*$^{+/-}$, but not *Pten*$^{+/+}$ mice, in parallel to a 2.5-fold increase in mRNA of Nkx3.1 (Figure 2B), a prostate-specific differentiation marker that is transcriptionally regulated by AR [21]. This occurs in the presence of normal plasma testosterone levels (Table 1).

2.4. High-calorie diet induces cell proliferation in *Pten*$^{+/-}$ prostate

Pten haplodeletion causes an increase in Akt and MAPkinase (MsAPK) activation in prostate tissue, as assessed by Western analysis of total lysates with α-phospho-Akt and α-phospho42/44 antibodies (α-pAkt and α-p42/44, respectively) (Figure 3A). This occurs in the absence of a significant effect on the basal phosphorylation of insulin receptor substrate1 (IRS1), as expected from the downstream effect of *Pten* deletion. HC feeding further induces Akt and MAPK phosphorylation by 2-fold in *Pten*$^{+/-}$, but not *Pten*$^{+/+}$ mice. Consistently, mRNA levels of β-catenin proto-oncogene, an Akt downstream target, are 3- to 4-fold

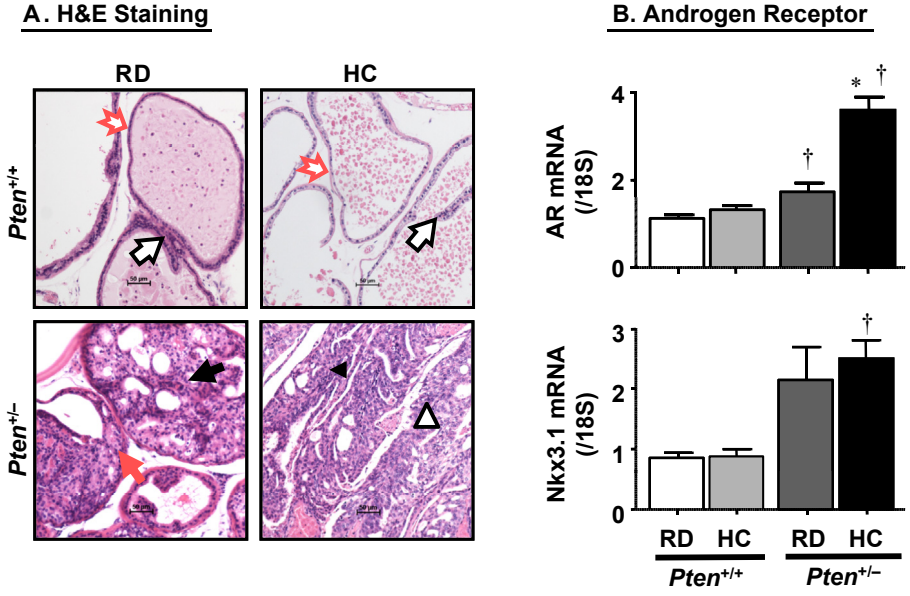

Figure 2: High-calorie diet causes neoplastic progression in *Pten*$^{+/-}$ prostate. One-month old mice were fed RD or HC for 6 months. (A) Ventral and dorsolateral lobes of the prostate were stained by H&E for histological analysis. The most progressive mPIN from each group was counted. *Pten*$^{+/+}$ shows features of mPIN 0-1 (hollow red arrow) and mPIN 1-2 (hollow black arrow). RD-fed *Pten*$^{+/-}$ exhibits predominantly mPIN 3 with extensive gland-in-gland proliferation inside the lumen (red arrow) and hyperchromatic nuclei (black arrow). HC-fed *Pten*$^{+/-}$ predominantly develops mPIN 4 with carcinoma *in situ* and more diffuse stromal invasion (black arrowhead). Some HC-fed *Pten*$^{+/-}$ mice show invasion of the basement membrane surrounding the gland (hollow arrowhead). Panels represent at least 14 mice per group. Magnification: 50 μm (20×). (B) mRNA levels of AR and its target, Nkx3.1, were analyzed by qRT-PCR, normalized to 18S and expressed as mean ± SEM (n = 6/group). *$p < 0.0125$ vs RD per mouse group and $^{\dagger}p < 0.0125$ vs same feeding regimen in *Pten*$^{+/+}$.

Table 2 — High-calorie diet induces mPIN progression.

	4 Months				7 Months			
	Pten$^{+/+}$		*Pten*$^{+/-}$		*Pten*$^{+/+}$		*Pten*$^{+/-}$	
	RD (n = 28)	HC (n = 24)	RD (n = 24)	HC (n = 25)	RD (n = 14)	HC (n = 27)	RD (n = 15)	HC (n = 14)
mPIN 1	4 (1)	8 (2)	4 (1)	0	30 (4)	14 (4)	0	0
mPIN 2	93 (26)	58 (14)	58 (14)	36 (9)	56 (8)	71 (19)	13 (2)	14 (2)
mPIN 3	4 (1)	29 (7)	37 (9)	52 (13)	15 (2)	14 (4)	73 (11)	64 (9)
mPIN 4	0	4 (1)	0	12 (3)	0	0	13 (2)	0
Invasion	0	0	0	0	0	0	0	21 (3)

Ventral and dorsolateral lobes of the prostate were excised from *Pten*$^{+/+}$ and *Pten*$^{+/-}$ mice fed either RD or HC for 3 or 6 months. mPIN lesions were scored in H&E stained sections by at least 2 certified pathologists. Numbers represent percentage per total mice examined per group. Numbers in parentheses represent absolute number of mice.

higher in RD-fed *Pten*$^{+/-}$ than *Pten*$^{+/+}$ mice (Figure 3B). They undergo a further 2-fold increase in mutant mice by HC feeding. Moreover, HC induces PCNA protein content by ~2-fold in *Pten*$^{+/-}$, but not *Pten*$^{+/+}$ mice, as demonstrated by Western analysis of prostate lysates with α-PCNA antibody (Figure 3C). Moreover, IHC analysis reveals elevation in Ki67 positive cells in prostate lesions with a higher mPIN in RD-fed *Pten*$^{+/-}$ as compared to RD-fed *Pten*$^{+/+}$ (Figure 3D, lower vs upper left panel, and corresponding graph), and a further 2-fold induction by HC feeding in *Pten*$^{+/-}$, but not *Pten*$^{+/+}$ mice (Figure 3D, lower vs upper right panel).

PI3K/Akt upregulates SOX9 expression and loss of *Pten* leads to elevated SOX9 levels, resulting in increased luminal cell proliferation and early high grade PIN lesions in mice [22]. Consistently, *Pten* haplodeletion causes a 4-fold increase in SOX9 mRNA levels (Figure 3E), and HC feeding further induces SOX9 mRNA levels by ~6-fold in mutant mice. IHC analysis reveals a predominant nuclear localization in lower mPIN as in RD-fed *Pten*$^{+/-}$ mice (Figure 3F, arrowhead). As mPIN progresses in *Pten*$^{+/-}$ mice upon HC feeding, cytoplasmic (Figure 3F, arrow) as well as nuclear localization of SOX9 occurs. This demonstrates that HC feeding activates the Akt-dependent cell survival cascade to enhance cell proliferation in *Pten*$^{+/-}$ prostate, in part by inducing cytoplasmic SOX9 expression, as has been reported [23].

The level of SNAIL transcription factor is elevated during epithelial—mesenchymal transition (EMT), which enhances cellular migratory/invasive properties to facilitate metastatic dissemination [24]. Consistently, Western and immunohistochemical (IHC) analyses (Figure 4A) indicate a significant HC-mediated induction of SNAIL protein levels in *Pten*$^{+/-}$, but not *Pten*$^{+/+}$ mice. In keeping with the repressive effect of SNAIL on E-cadherin [24], immunostaining analysis reveals a prominent heterogenous expression of E-cadherin in HC-fed *Pten*$^{+/-}$ (Sup Figure 2A, arrow in lower right panel). In contrast, N-Cadherin protein level increases significantly in HC-fed compared to RD-fed *Pten*$^{+/-}$ mice and their wild-type littermates (Sup Figure 2B, arrow in lower right panel).

2.5. High-calorie intake increases angiogenesis in *Pten*$^{+/-}$ prostate

Prostate tumor exhibits an increase in vascular density due to elevated angiogenesis [25]. Accordingly, IHC analysis reveals a more diffuse immunostaining of CD31 endothelial cell marker in HC-fed relative to RD-*Pten*$^{+/-}$ and wild-type mice (Sup Figure 3, lower right panel vs others). Moreover, *Pten* haplodeletion causes a 2—3 fold increase in the mRNA levels of factors involved in regulating endothelial and vascular integrity, such as angiopoietin1 (Ang1) and VE-cadherin (Sup Table 2). Consistent with loss of *Pten* and subsequent Akt-mediated induction of hypoxia inducible factor-1α (HIF1α) that constitutes an early event in prostate carcinogenesis [26], mRNA levels of HIF1α are 4-fold higher in RD-fed *Pten*$^{+/-}$ and they undergo further induction by HC feeding in *Pten*$^{+/-}$ but not *Pten*$^{+/+}$ mice (Sup Table 2).

In agreement with the pro-angiogenic role of the carcinoembryonic antigen-related cell adhesion molecule (CEACAM1) [27], Western analysis shows a marked elevation in its protein content in *Pten*$^{+/-}$ prostate, in particular upon HC feeding (Figure 4B). Double immunostaining with CEACAM1 (red) and CD31 (brown) antibodies reveals normal localization of CEACAM1 in epithelial cells lining the lumen of prostate glands in RD-fed wild-type and RD-fed mutant mice (Figure 4C, left panels, arrows). CEACAM1 is also detected in some endothelial cells in RD-fed mutant mice (Figure 4C, lower left panel, arrowheads). In parallel to progressive neo-vascularization, HC feeding causes a concomitant detection of CEACAM1 in endothelial cells lining blood vessels (Figure 4C, arrowheads), with a marked decrease in its expression in epithelial cells, especially in mutant mice with mPIN 4 and higher, as has been previously shown in humans with high Gleason score [28].

2.6. High-calorie diet provokes inflammation in *Pten*$^{+/-}$ prostate

Cancer is often associated with inflammatory infiltration. Consistently, immunostaining analysis reveals elevation in the stromal infiltration of inflammatory cells such as macrophages (F4/80), T-cells (CD4/CD8), T-regulatory cells (FoxP3), and inflammatory monocytes (Gr1-R) in the prostates of RD-*Pten*$^{+/-}$ compared to RD-fed wild-types (Figure 5). HC induces a further increase in these inflammatory cells to a larger extent in *Pten*$^{+/-}$ than wild-types (Figure 5). The higher inflammatory response to HC in *Pten*$^{+/-}$ mice is supported by elevation in the expression of CD3, CD45, FoxP3, chemokines (such as the monocyte chemoattractant protein 1, MCP1) and cytokines (such as interleukin 6, IL6 and TNFα) (Sup Table 3). Taken together, this demonstrates that loss of *Pten* cooperates with HC diet to induce inflammation in prostate.

2.7. High-calorie intake induces fatty acid synthesis in *Pten*$^{+/-}$ prostate

In *Pten*$^{+/-}$ but not *Pten*$^{+/+}$ mice, HC feeding induces mRNA levels of peroxisome proliferator-activated receptor (PPARγ) and sterol regulatory element binding proteins (SREBP1c) (Figure 4D), a master regulator of lipogenic genes, such as FAS, a downstream target of MAPK and Akt pathways [8]. Consistently, immunostaining analysis reveals a more intense FAS staining in the epithelial cells of prostates from HC-fed *Pten*$^{+/-}$ mice (Figure 4E, lower right vs other panels, arrows). With FAS acting as a key energy source for proliferating cancer cells [29,30], the data suggest that increased cell proliferation in prostates derived from HC-fed *Pten*$^{+/-}$ mice could be associated with increased FAS content (see below).

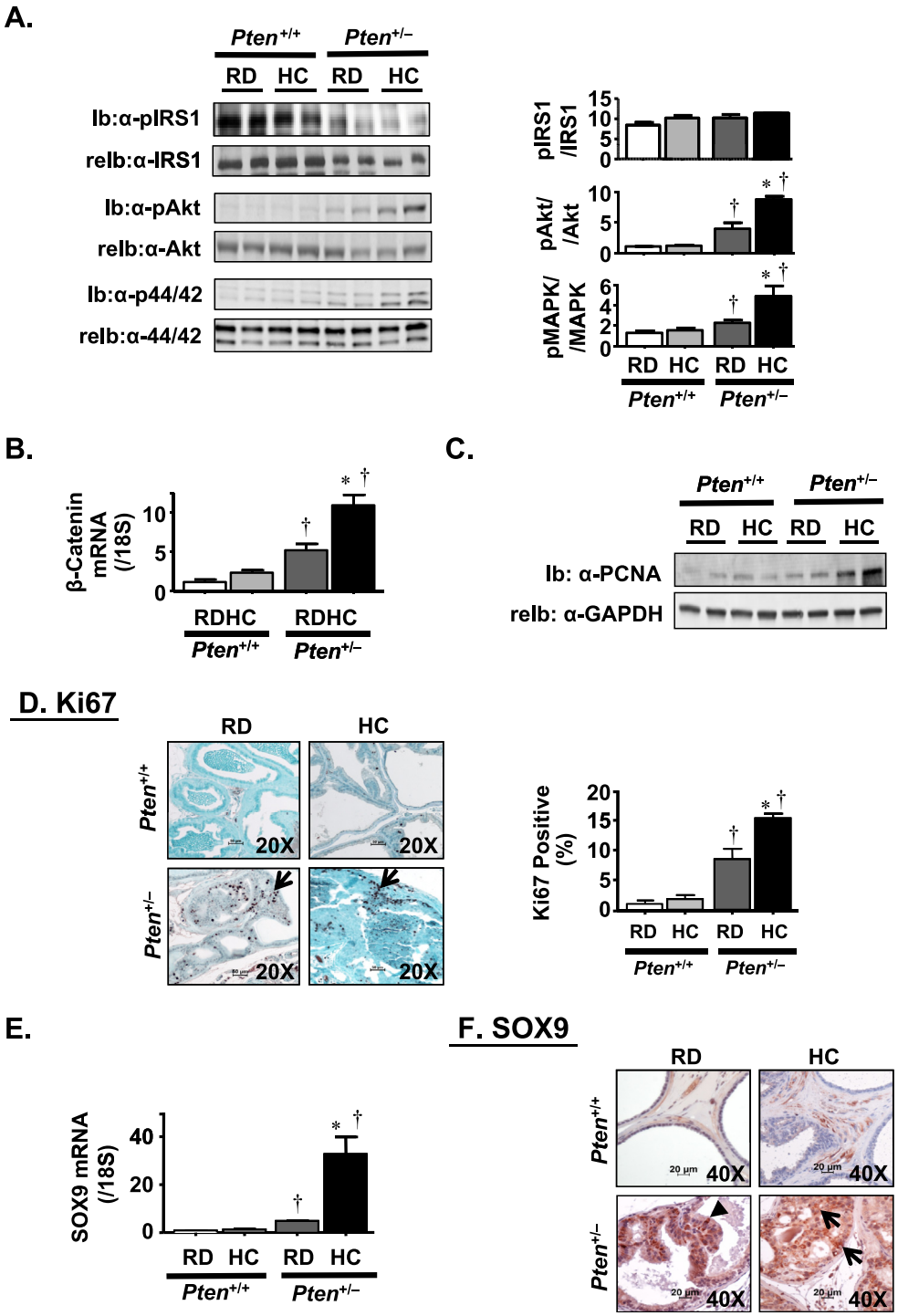

Figure 3: High-calorie diet induces cell proliferation in *Pten*$^{+/-}$ prostate. (A) Proteins were analyzed by Western blot analysis using antibodies against α-phospho-IRS1, α-phospho-Akt and α-phospho-p44/p42 (MAPK) for immunoblotting (Ib) followed by reprobing (re-Ib) with α-IRS1, α-Akt and α-p44/p42, respectively. Density of phosphorylated bands was measured relative to total proteins in arbitrary units, and represented in the bar graphs. Gels represent at least 3 different experiments performed on different sets of mice. (B) qRT-PCR analysis of mRNA of β-catenin normalized to 18S and expressed as mean ± SEM (n = 6/group). (C) Western analysis of PCNA protein levels, normalized against α-GAPDH, as above. (D) Ki67 staining (n ≥ 5/group). Magnification: 50 μm (20×). Bar graph represents percentage of Ki67 positive relative to total cells in at least 500 cells. (E) qRT-PCR analysis of SOX 9 (n ≥ 5 mice/group), expressed as mean ± SEM. In *A–E*, $^{*}p < 0.0125$ vs RD per mouse group and $^{\dagger}p < 0.0125$ vs same feeding regimen in *Pten*$^{+/+}$. (F) Immunohistochemical analysis of SOX 9 (n ≥ 5/group). Magnification: 20 μm (40×).

2.8. Insulin induces cell proliferation, migration and tumorigenicity in human prostate cells with PTEN loss

To investigate whether the rise in insulin plays a role in mediating neoplastic progression, PTEN was knocked down in RWPE-1 normal human prostate epithelial cells using siRNA against PTEN (siPTEN) or scrambled controls (Scr) (Figure 6A) and treated with low (100 nM) (Figure 6B) or high (1 μM) (Figure 7A) levels of insulin before cell growth was determined by MTT assay. As Figures 6B and 7A show,

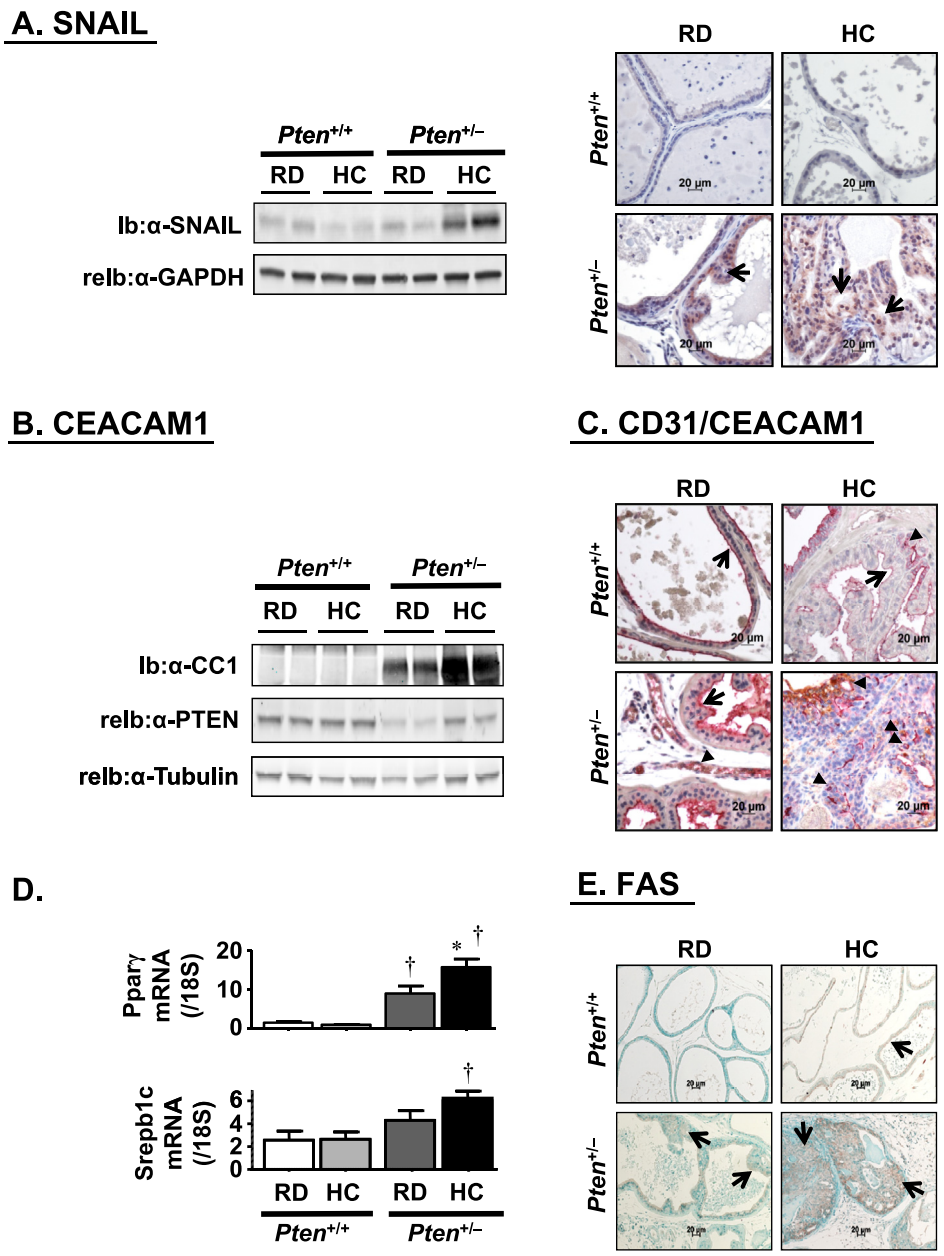

Figure 4: High-calorie diet causes EMT, angiogenesis and lipogenesis in *Pten*$^{+/-}$ prostate. (A) SNAIL analysis by Western blotting and immunostaining with antibodies against α-SNAIL antibody. Gels represent at least 3 different experiments performed on different sets of mice. (B) Western analysis with α-CEACAM1 followed by PTEN and tubulin antibodies, as above. (C) Immunohistochemical analysis with α-CD31 (brown) and α-CEACAM1 (red) antibodies (n ≥ 5/group). Arrows refer to epithelial expression and arrowheads to endothelial localization of CEACAM1. (D) qRT-PCR analysis of PPARγ and SREBP1c, as above. mRNA values are expressed as mean ± SEM (n = 6/group); *$p < 0.0125$ vs RD per mouse group and †$p < 0.0125$ vs same feeding regimen in *Pten*$^{+/+}$. (E) Immunohistochemical analysis of FAS (n ≥ 4/group). Magnification: 20 μm (40×).

insulin induces cell growth in both cells, but by >2- to 3-fold higher level in siPTEN cells (black vs light gray bars). This occurs in parallel to a ~2-fold stronger insulin-induced Akt phosphorylation in these knockdown cells (Figure 6B, Western blot). In contrast, blocking Akt phosphorylation by Akti-1/2 inhibitor reduces markedly cell growth in response to insulin (Figure 6B, hatched vs solid bars) without affecting IRS-1 phosphorylation in both groups of cells (Figure 6B, Western blot). Together, this shows that Akt activation is a main mediator of the superior effect of insulin on cell growth in siPTEN- relative to scrambled-transfected cells.

Treatment with 10 nM Insulin for 5 h significantly increases cell migration in siPTEN cells, whereas scrambled siRNA-expressing cells are non-migratory in response to insulin (Figure 7B). We further tested whether insulin increases anchorage-independent growth of prostate epithelial cells with PTEN knockdown by performing soft agar colony formation assays. Consistent with increased cell proliferation, treatment with insulin (1 μM) for three weeks significantly increases the number of small and medium sized colonies on soft agar in RWPE-1 with siPTEN (Figure 7C). Of note, mRNA and Western analysis reveal 50% loss of PTEN after 3 weeks, simulating the haploinsufficiency state in mice.

Moreover, insulin (1 μM) elevates the mRNA levels of Bv8 (prokineticin 2) in RWPE-1 cells with 50% loss of PTEN (Figure 8A) without affecting VEGF (1.11 ± 0.00 vs 0.86 ± 0.05 in siPTEN and

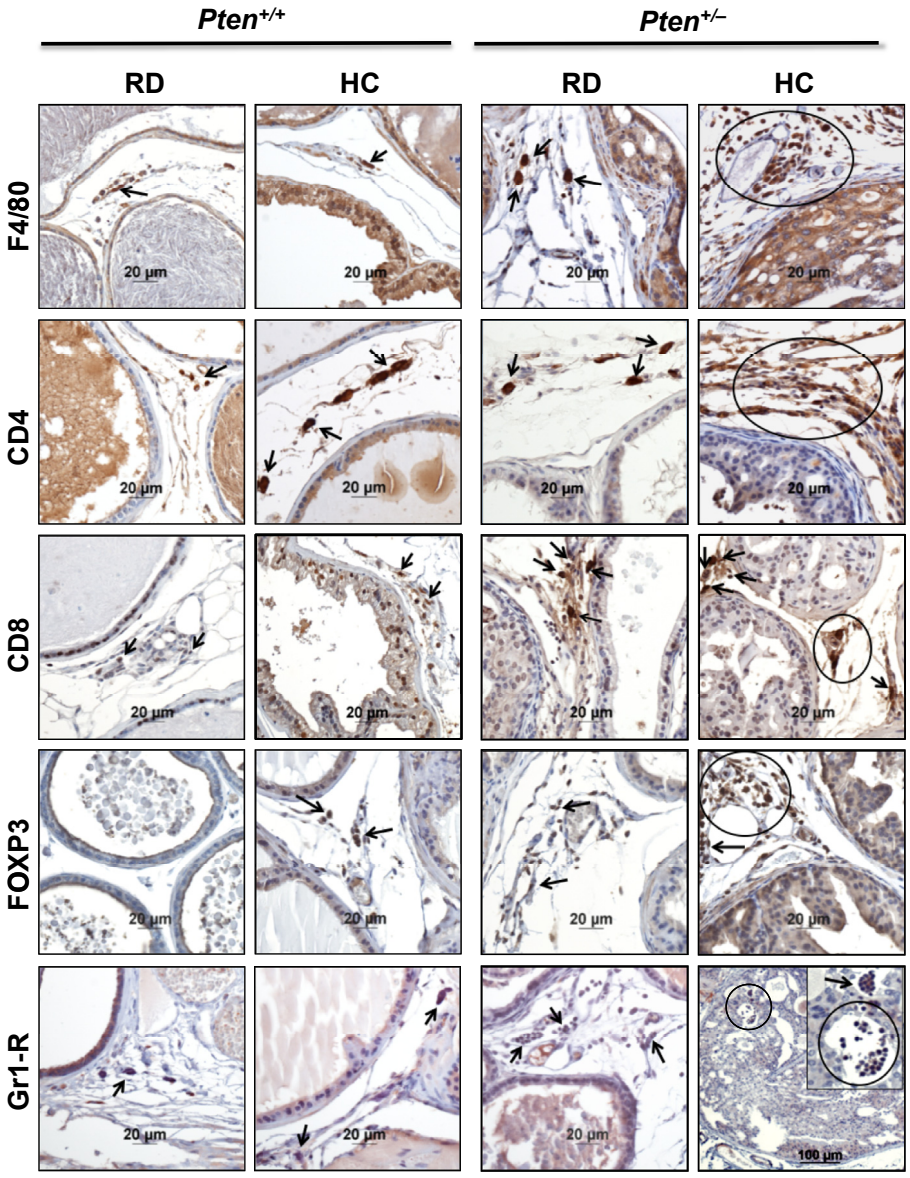

Figure 5: High-calorie diet induces inflammation in *Pten*$^{+/-}$ prostate. Immunohistochemical analyses of F4/80, CD4, CD8, FoxP3 and Gr1-R ($n \geq 5$/group). All exposures shown are at 20 μm (40×), except for Gr1-R staining in HC-fed mutant, at 100 μM (10×), with the inset at 20 μm (40×) to highlight inflammatory cells.

1.23 ± 0.07 vs 1.00 ± 0.03 in scrambled), consistent with a permissive role for Bv8 in cell proliferation independently of VEGF [31]. PTEN down-regulation elevates SOX9 mRNA, and consequently, that of its target, CEACAM1, which is further induced by insulin treatment, as expected from insulin-induced transcriptional activity of Ceacam1 promoter [32]. Although not statistically significant, insulin tends to induce mRNA of human kallikrein 2 (KLK2), a prostate-specific peptidase that reduces cell apoptosis, in siPTEN cells (2.78 ± 0.31 vs 1.96 ± 0.19 in siPTEN and 1.19 ± 0.14 vs 1.27 ± 0.09 in scrambled).

As expected [33], mRNA of FAS is increased by PTEN down-regulation, and undergoes further stimulation by insulin (Figure 8A). Down-regulating FAS by ~60% in siPTEN-cotransfected cells (Figure 8B, *i*) markedly blunted the positive effect of insulin on cell growth in response to insulin, not only by comparison to siPTEN cells (Figure 8B, *ii* dotted vs black bar), but also to Scr cells (dotted vs light gray bar). This assigns a critical role for FAS induction in insulin-mediated increase in cell growth.

2.9. IL-6 induces cell proliferation in human prostate cells with PTEN loss

Because IL-6, an independent risk factor in the progression of prostate cancer [34], is elevated in HC-fed *Pten*$^{+/-}$ mice (Sup Table 3), we then tested whether it induces growth of siPTEN-transfected RWPE-1 cells. As Figure 8B shows, IL-6 promotes cell growth more strongly in siPTEN than scrambled cells (blue vs purple bars) and that this effect is markedly reduced with additional loss of FAS (patterned blue hatchings vs blue bars) to reach the level induced by IL-6 in scrambled cells (patterned blue hatchings vs purple bars). This suggests that FAS elevation plays an important role in mediating the inflammatory effect of PTEN downregulation. While the growth effect of IL-6 is much less pronounced than that of insulin in all cell types, the combined

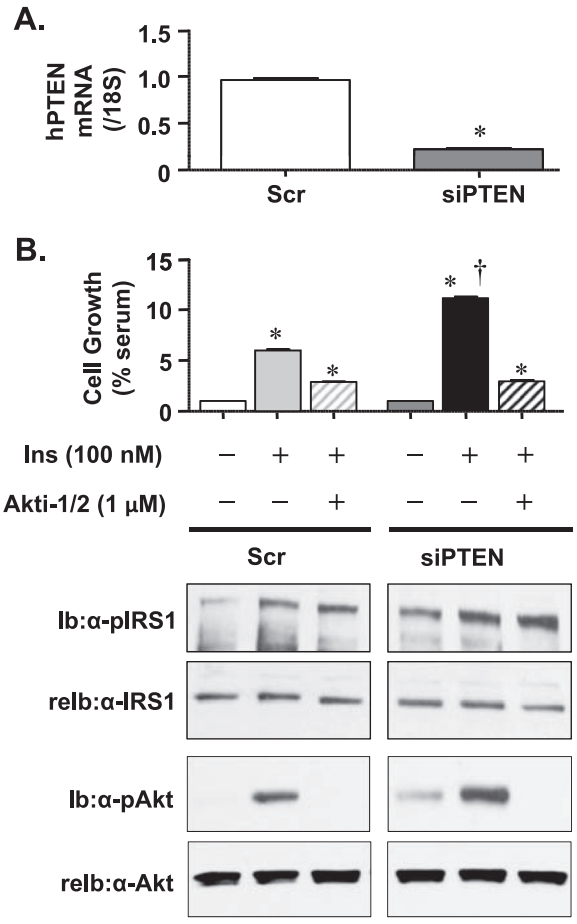

Figure 6: Insulin stimulates cell growth in RWPE-1 human prostate epithelial cells in an Akt-dependent manner. (A) Cells were transfected with scramble (Scr) or siPTEN and their mRNA analyzed by qRT-PCR to determine PTEN levels. $*p < 0.0125$ vs Scr. (B) In MTT assays (graph), cells were treated with either complete medium (maximal growth) or growth factor-free medium (basal growth) that was supplemented in some cells with 100 nM insulin in the presence or absence of Akti-1/2 inhibitor for 48 h and counted. Cell growth was calculated as percentage of maximal growth (cell number in the presence of insulin minus basal growth divided by cell number in complete medium × 100). Experiments were performed in triplicate and repeated at least three times. $*p < 0.0125$ vs untreated and $^{\dagger}p < 0.0125$ vs same treatment group in Scr. In parallel experiments, Western analysis was performed to examine IRS-1 and Akt phosphorylation. Gels represent at least 3 experiments.

treatment with IL-6 and insulin causes a synergistic effect in both scrambled and siPTEN cells.

3. DISCUSSION

Diet-induced obesity is associated with increased risk for prostate cancer [2]. The molecular interplay between dietary and genetic factors in prostate cancer progression remains elusive. Recent studies have shown that *PTEN* is the most commonly lost tumor suppressor gene in prostate cancer in men [14]. As in humans, monoallelic deletion of *Pten* gene in mice causes localized non-malignant mPIN lesions [16]. The current studies demonstrate that HC feeding drives an accelerated onset and progression of a more malignant neoplastic phenotype in haploinsufficient $Pten^{+/-}$ mice in association with stromal reactivity, angiogenesis and EMT. This provides an *in vivo* evidence of a permissive role for a hypercaloric diet in prostate cancer progression in these genetically predisposed mice.

Consistent with previous findings [17,19], *Pten* deficiency enhances insulin signaling through the PI3K/Akt pathway *in vivo* and in cells with PTEN downregulation. HC feeding elevates insulin levels in $Pten^{+/-}$ mice, albeit to a lesser extent than their wild-type littermates. Together with absence of lipolysis, this modest rise in insulin level is consistent with a relatively more protected insulin response in *Pten* mutants [18,35]. As with *Pten* haploinsufficiency, constitutive activation of Akt does not cause spontaneous invasive carcinoma or metastasis in MPAKT mice fed a regular chow diet [36]. This supports the notion that *Pten* haplodeletion alone does not suffice to promote invasive prostate carcinoma, and points to altered metabolic parameters as key mediators of the neoplastic progression in HC-fed $Pten^{+/-}$ mice.

Insulin affects cell proliferation, migration and invasion through both PI3K/Akt and Ras/MAPK signaling pathways. The current studies reveal that insulin markedly induces cellular migration and proliferation, and colony formation on soft agar in RWPE-1 normal human prostate epithelial cells in which PTEN is markedly reduced. Mechanistically, this could be mediated by insulin's induction of several factors involved in regulating cell proliferation, growth, adhesion and motility, including CEACAM1 [27] and FAS [8]. Thus, hyperinsulinemia may play an important role in promoting prostate cancer cell motility in HC-fed $Pten^{+/-}$ mice, which manifest more insulin sensitivity than HC-fed $Pten^{+/+}$ mice.

Progressive prostate carcinogenesis in HC-fed $Pten^{+/-}$ mice is accompanied by an increase in SNAIL and N-Cadherin expression with a reciprocal reduction in E-Cadherin. Akt activation could mediate EMT through E-Cadherin repression by SNAIL [37]. Additionally, induced CEACAM1 expression by insulin [32], and/or by activating SOX9 [38] and androgen receptor [39], could play a role in this process. Because overexpressing CEACAM1 reduces the adhesive properties of HT29 colorectal carcinoma and 293T cells via upregulating N-Cadherin [40], it is possible that induction of CEACAM1 and N-cadherin regulate cancer cell motility in HC-fed $Pten^{+/-}$ mice.

Consistent with neo-vascularization playing a key role in cancer metastasis [41], HC feeding increases the intraepithelial neovascularization in $Pten^{+/-}$ but not wild-type mice. This may result, at least partly, from elevated expression of angiogenic factors, such as HIF1α, SOX9 and CEACAM1. While SOX9 transcription factor plays a key role in the growth and development of normal prostate, increases in its levels correlate positively with advanced Gleason score and tumor progression in human prostate tumor [22]. Moreover, SOX9 could synergize with insulin to upregulate CEACAM1 expression in endothelial cells, leading to intratumoral angiogenesis and vascular maturation in HC-fed $Pten^{+/-}$ mice [42].

Prolonged HC feeding causes infiltration of inflammatory cells that contribute to altered metabolic abnormalities [43] as well as tissue reorganization during tumor growth [44]. Among the several pro-inflammatory factors that are induced in $Pten^{+/-}$ mice is IL-6, a cytokine that constitutes an independent risk factor in prostate cancer progression [34]. In siPTEN-cells, IL-6 alone induces cell growth, albeit to a lower extent than insulin, but also synergizes with this growth factor to cause a more robust proliferative effect than insulin alone. Given that PTEN exerts an anti-inflammatory effect [45], this suggests that IL-6 synergizes with insulin's amplification of PI3K/Akt activation by *Pten* loss to contribute to the progression of prostate neoplasia in HC-fed $Pten^{+/-}$ mice, as has been shown in humans and rodents [46]. Moreover, HC feeding induces the Foxp3+Treg pool that is positively associated with advancement of tumor stage [47]. Together, the data suggest that HC induction of an inflammatory response contributes to the neoplastic progression in HC-fed $Pten^{+/-}$ mice.

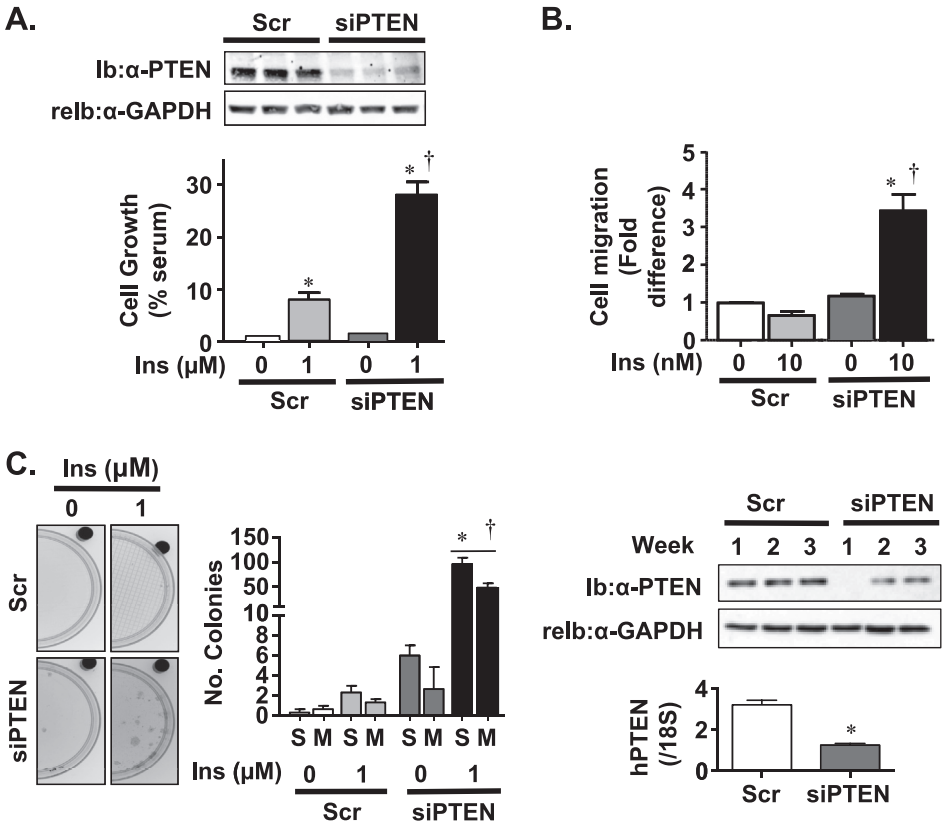

Figure 7: Insulin stimulates cell growth, migration and colonization in RWPE-1 cells. (A) Cells were transfected with Scr or siPTEN and analyzed by Western blot to confirm reduction in PTEN levels. In MTT assays, cell growth in response to insulin (1 μM) was performed as in the legend to Figure 6. Experiments were performed in triplicate and repeated at least three times. (B) Cells were treated with or without insulin (10 nM) for 5 h and cell migration assessed by measuring the fluorescence units of cells migrated into the clearing zone. (C) Cells were plated on 0.7% soft agar, cultured in growth factor free media supplemented with 0.1% BSA either alone or with 1 μM insulin for 21 days. The bar graph represents the number of colonies on the soft agar categorized as small and medium colonies based on the cell number per colony. In a parallel experiment, knockdown efficiency was assessed by Western blot weekly and by mRNA analysis after 21 days. Experiments were performed in triplicate and repeated at least twice. In A–C, $^{*}p < 0.0125$ vs untreated and $^{\dagger}p < 0.0125$ vs same treatment group in Scr.

Consistent with the inverse correlation between FAS and PTEN in human prostate cancer [48], HC feeding markedly induces FAS level in *Pten*$^{+/-}$ mice. Enhanced *de novo* synthesis of fatty acids is positively associated with progressive prostate cancer in humans and mice [49], partly because fat accumulation promotes a pro-inflammatory cellular milieu [50]. In contrast, anti-FAS therapy limits prostate cancer progression [51]. Insulin's stimulation of FAS in PTEN knockdown RWPE-1 cells suggests that increased FAS expression in HC-fed *Pten*$^{+/-}$ mice is likely mediated by insulin-induced SREBP1c activation, which can occur in both insulin sensitive and insulin resistance states [33]. Reversal of the proliferative effect of insulin (and IL-6) with the loss of FAS in siPTEN-cells indicates that FAS induction plays a key role in insulin- as well IL-6-mediated increase in cell growth. This points to fatty acid synthesis as a key molecular player linking diet-induced lipogenesis to cell proliferation and inflammation during prostate cancer progression in HC-fed *Pten*$^{+/-}$ mice.

The regulatory role of PTEN-dependent regulation of lipogenesis in prostate cancer progression has been recently emphasized by the demonstration that PTEN loss and PI3K/Akt activation cause cholesterol ester accumulation that leads to aggressiveness of human prostate cancer [52]. Although like insulin, plasma cholesterol and triglyceride levels did not correlate significantly with mPIN score, we cannot rule out a potential role for these metabolic parameters in HC-induced neoplastic progression in *Pten*$^{+/-}$ mice, either synergistically with insulin or individually. More studies are needed to further explore this possibility.

The current studies provide an *in vivo* demonstration that HC promotes prostate cancer progression in a model of genetic susceptibility resulting from loss of *Pten*, a well-characterized tumor suppressor gene. Mechanistically, this advanced neoplastic state (including angiogenesis, EMT and inflammation), could be mediated, at least in part, by enhanced activation of Akt and MAPK pathways and induction of *de novo* lipogenesis in prostate (as predicted from elevated FAS) in the presence of enhanced insulin response to chronically elevated insulin levels. The high incidence of *PTEN* haploinsufficiency in prostate cancer in men underscores the therapeutic impact of our observations, particularly in light of the epidemic spread of diet-induced obesity in the industrialized world.

4. METHODS

4.1. Animals

Pten^{tm1Rps} mice [20], backcrossed onto the C57BL/6 (BL6) background were obtained from the National Cancer Institute's Mouse Models of Human Cancers Consortium. All mice were kept in a 12-h dark/light cycle. All procedures were approved by the Institutional Animal Care and Utilization Committee.

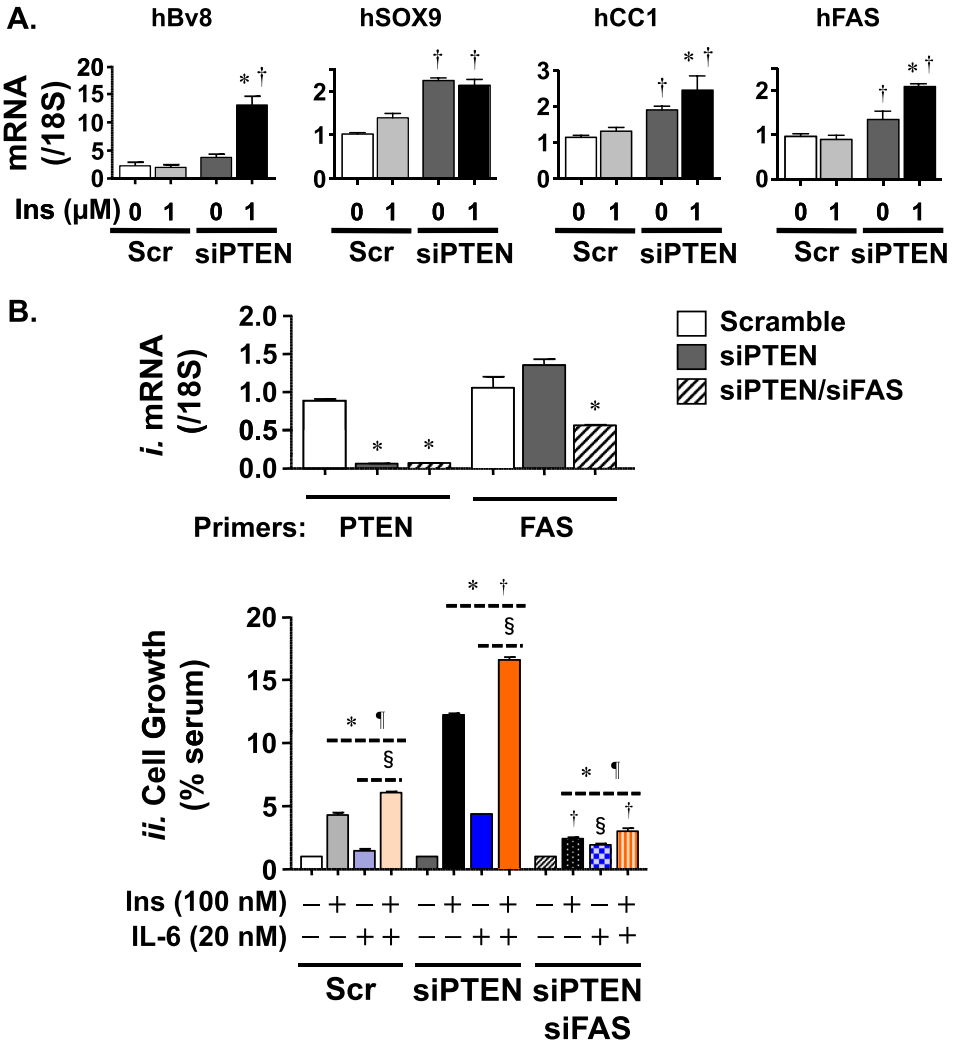

Figure 8: Effect of fatty acid synthase on insulin- and IL-6-mediated cell growth in RWPE-1 cells. (A) Scr- and siPTEN-transfected cells were treated with or without insulin (1 μM) in parallel to transfection in Figure 7A, before mRNA was analyzed by qRT-PCR. Experiments were performed in triplicate and repeated at least twice. *$p < 0.0125$ vs untreated and $^{\dagger}p < 0.0125$ vs same treatment group in Scr. (B) Cells were transfected with Scr, siPTEN and siPTEN + siFAS, and their PTEN and FAS levels were determined by qRT-PCR, using specific primers (*i*). Cells were treated with buffer, insulin (100 nM), IL-6 (20 nM) or insulin and IL-6, before cell growth was assessed by MTT (*ii*). *$p < 0.0125$ vs untreated per each cell group, $^{\dagger}p < 0.0125$ vs same treatment group in Scr, $^{\S}p < 0.0125$ vs insulin in each cell group, and $^{\P}p < 0.0125$ vs same treatment group in siPTEN.

4.2. Mouse feeding

At weaning (one month of age), mice were fed *ad libitum* either a standard chow (RD) (Teklad® 2016), deriving 12% of calories from fat, 66% from carbohydrate and 22% from protein or a high-calorie diet (HC) deriving 45% of calories from fat, 35% from carbohydrate and 20% from protein (Research Diets, Inc., New Brunswick, NY, Catalog #D12451). The dietary fat composition of HC is 36.3% saturated; 45.3% monounsaturated fatty acids, and 18.5% polyunsaturated fatty acids.

4.3. Metabolic analysis

Following an overnight fast, mice were anesthetized with sodium pentobarbital (55 mg/kg body weight), and whole venous blood was drawn from retro-orbital sinuses to measure fasting glucose levels using a glucometer (Accu-chek® Aviva; Roche® Diagnostics, Indianapolis, IN). Plasma insulin and C-peptide levels were measured by radioimmunoassays (Millipore, St. Charles, MO), non-esterified fatty acids (NEFA) by NEFA C kit (Wako Diagnostics, Richmond, VA), triglycerides by a kit from Pointe Scientific (Canton, MI), and testosterone by a kit from Endocrine Technologies (Newark, CA). Visceral adiposity was expressed as % of epididymal plus intestinal white adipose tissue per total body mass.

4.4. Histopathology and phenotyping of prostate lesions

Formalin-fixed ventral and dorsolateral lobes of prostate were embedded in paraffin blocks and serially sectioned to 5 μm thickness. Some sections were stained with hematoxylin & eosin (H&E) and analyzed for prostatic intraepithelial neoplasia (mPIN) by two independent certified pathologists (P.C. and C.G-W.), using the classification scheme of Cardiff and colleagues [53]. Accordingly, mPIN was classified into four levels (mPIN 1-4) based on micro-architecture, differentiation pattern and degree of nuclear atypia, with mPIN 4 being the most progressive form, but differing from invasive carcinoma by retaining an intact basement membrane surrounding the prostate gland. One score was assigned for each mouse based on the worst lesion observed on a single H&E section.

4.5. Immunohistochemistry

Sections were baked at 60 °C for 1 h prior to hydration in alcohol and water and treatment with Antigen Retrieval solution (Vector Laboratories Inc., Burlingame, CA), followed by quenching with H_2O_2 for 30 min. Using the VECTASTAIN Elite ABC PEROXIDASE kit PK-6101 and vector MOM immunodetection PEROXIDASE kit PK-2200 (Vector Laboratories), sections were incubated overnight at 4 °C in primary antibodies diluted in MOM™ diluent provided with the kit. Antibodies include: α-Ki67 (1:50, monoclonal, BD Pharmingen, NJ, USA), α-FAS (1:50, polyclonal, Enzo Life Sciences, Plymouth Meeting, PA), α-CD31 (1:20, monoclonal, DAKO, Germany), α-SOX9 (1:50, polyclonal, Santa Cruz Biotech, Santa Cruz, CA), α-SNAIL (1:100, polyclonal, Abcam, Cambridge, MA), α-E-Cadherin (1:150, monoclonal, Cell Marque Rocklin, Cell Marque Rocklin, CA), α-N-Cadherin (1:50, polyclonal, Abcam), F4/80 (1:50, polyclonal, Abcam), FoxP3 (1:100, polyclonal, Abcam), CD4 (1:50, monoclonal, Abcam), CD8 (1:50, monoclonal, Lifespan Biosciences, Seatle, WA) and Gr1-R (1:10, monoclonal, BD Biosciences, San Jose, CA). On the next day, the secondary antibody was added and sections were washed for visualization with the Vector® NovaREDTM Substrate Kit (SK-4800) and DAB Peroxidase Substrate Kit (SK-4100) following manufacturer's instructions. Double-immunostaining was performed with antibodies against α-CEACAM1 (1:500, Ab-2457-a custom made rabbit polyclonal) and α-CD31, using Picture Plus double staining (DS 87-9999) kit from Invitrogen (Camarillo, CA).

4.6. Western blot analysis

35 μg of protein lysates from the anterior prostate lobe of overnight fasted age-matched mice was separated using 4–12% SDS-PAGE (Invitrogen). Proteins were immunoblotted (Ib) with polyclonal antibodies against CEACAM1 (as above), α-PCNA (Santa Cruz Biotechnology), α-phospho-p44/42(pMAPK), α-p44/42(MAPK), α-phosphoSer 473 Akt, α-Akt, α-PTEN and α-SNAIL (all from Cell Signaling Technology, Denvers, MA) followed by reprobing (relb) with monoclonal antibody against GAPDH or tubulin (Santa Cruz Biotechnology) to normalize for total protein content. Proteins were detected using LiCOR secondary antibodies according to manufacturer's instructions (LiCOR Biosciences, Lincoln, BE) and the protein band density was measured using Image J software and calculated as percentage of the amount of proteins loaded.

4.7. MTT assay

RWPE-1 (normal human prostatic epithelial cells) were cultured in Keratinocyte serum-free media (K-SFM) supplemented with epidermal growth factor and bovine pituitary extract (GIBCO Life Technology, Grand Island, NY). For MTT assay, 1×10^6 RWPE-1 cells were nucleofected with 40 pmol of either scrambled (Invitrogen, Catalog # 12935) or validated stealth siRNA-PTEN (Sense: AUUGUCAUCUUCACUUAGCCAUUGG; Antisense: CCAAUGGCUAAGUGAAGAUGACAAU; Invitrogen, Catalog # VHS41285), in the presence or absence of 60 pmol of validated stealth siRNA-FAS (Sense: 5′-CAGAGUCGGAGAACUUGCAGGAGUU-3′; Antisense: 5′-UUCTCCTGCUUGTTCTCCGUCTCTG-3′; Invitrogen; Catalog # FASN 1299001, RefSeq NM_004104) using either Lipofectamine 2000 (Invitrogen) or Nucleofector™ Kit R (Lonza, Basel, Switzerland). 48 h post-transfection, some cells were switched for 12–16 h to basal medium (serum-free and growth factor-free medium supplemented with 25 mM Hepes and 1% insulin-free BSA), before adding insulin (100 nM or 1 μM) and/or IL-6 (20 nM) (Recombinant Human IL-6, PeproTech Rocky Hill, NJ) for 48 h before being subjected to MTT assay (Sigma–Aldrich, St Louis, MO) and their absorbance read at 570 nm in 96-well plates. In some experiments, 1 μM of Akt-1/2 Kinase-inhibitor (Akti-1/2) (Sigma–Aldrich) was added 30 min before insulin treatment started. Cell growth was calculated as percent of growth in the presence of effector minus basal growth divided by maximum growth in complete medium. Of note, transfecting with 30–40 pmol of siPTEN yielded a similar ~70% decrease in PTEN expression, as opposed to 20 pmol that failed to reduce PTEN expression.

4.8. Migration assay

RWPE-1 cells in 10 cm plate were transfected with 300 pmol scrambled or siPTEN using Lipofectamine 2000 for 24 h. Cells were then trypsinized, stained with Calcein AM-FITC (Invitrogen) and seeded in Oris fibronectin coated 96-well plates with cell stoppers (Platypus Technologies, Madison, WI) and allowed to adhere. Stoppers were then removed and cells treated with insulin (0–1 μM) at 37 °C for 0–5 h. Fluorescence units were measured with a fluorescent plate reader using excitation at 488 nM and emission at 535 nM. Migration was calculated by the difference in the fluorescent units in insulin-treated and untreated cells.

4.9. Soft agar clonicity assay

RWPE-1 cells were plated in 10 cm plates, transfected and incubated for 24 h, as above. Cells were then trypsinized, counted and resuspended in growth factor-free K-SFM supplemented with BSA alone or with 1 μM insulin. 1×10^4 RWPE-1 cells were mixed with 0.7% DNA-grade agarose (prepared in sterile, cell culture grade 1× PBS, pre-boiled and cooled down to 40 °C) and layered on top of a 0.8% base agar layer. Plates were then incubated at 37 °C in humidified incubator for three weeks. Cells were fed with growth factor-free K-SFM media supplemented with BSA alone or with 1 μM insulin twice a week. On day 21 post-plating, the number of colonies was counted, and classified as small and medium based on the cell number per colony. To test the knockdown efficiency throughout this time, a parallel transfection with either scrambled siRNA or siPTEN was performed, and PTEN levels were analyzed by Western blot and qRT-PCR at the end of each week for three weeks.

4.10. Semi-quantitative real-time PCR

Total RNA was extracted from the anterior lobe of prostate or from RWPE-1 cells using PerfectPure RNA Tissue Kit (5 Prime, Gaithersburg, MD) according to manufacturer's protocol. 1 μg of total RNA was reverse-transcribed using iScript™ cDNA synthesis kit (Bio-Rad Laboratories, Herculus, CA) and the mRNA expression of individual genes was analyzed by semi-quantitative real-time PCR (qRT-PCR) in triplicate or quadruplet (Step One Plus Real time PCR system, Applied Biosystems, Foster city, CA) using gene specific primers as listed in Sup Table 1. The relative amount of mRNA of individual gene was calculated after normalizing to corresponding 18S and the results are expressed as fold change relative to *Pten*$^{+/+}$ on RD or Vehicle-treated control RWPE-cells.

4.11. Statistical analysis

Data were analyzed by two-way analysis of variance (ANOVA) using SAS statistical analysis software (SAS Institute, Inc, Cary, NC) and also by unpaired two-tailed Student t-test with GraphPad Prism software. $p < 0.0125$ was statistically significant. Spearman Correlation was used to compare mean of plasma insulin, cholesterol and triglycerides among all levels of mPIN, since mPIN is an ordinal variable scored from 1 to 4 and invasion.

AUTHOR CONTRIBUTIONS

J.L., S.K.R., M.K.K., S.S.K researched and analyzed data, and contributed to the drafting of the article. S.G.L., H.T.M., S.J.L., L.V.F.,

and A.J.K. researched data. I.E.M., and C.G-W. contributed to discussion. C-G-W and P.B.C. are certified pathologists that scored histology independently. K.M.E. contributed to the design of the in vitro data and contributed to the discussion. S.M.N. oversaw the work, including its conception and study design, analyzed data, led scientific discussions and wrote/reviewed/edited the manuscript.

ACKNOWLEDGMENTS

The authors thank Melissa Kopfman and Jennifer Kalisz at the Najjar laboratory for excellent technical assistance. They also thank Dr. Sadik A. Khuder for invaluable help in statistical analysis and Drs. Edwin R. Sanchez, Steven H. Selman, Kam C. Yeung, Han-Fei Ding, Baochun Zhang, Zhe Wang, and Terry Hinds from the University of Toledo, College of Medicine and Life Sciences for helpful scientific discussions. This work is supported by grants from the National Institutes of Health (R01 DK054254, R01 DK083850 and R01 HL112248 (S.M.N.) and R01CA151632 (K.M.E.), the U.S. Department of Agriculture (38903-19826) (S.M.N), the University of Toledo Foundation (K.M.E.), the Hiss Fund (I.E.M and C.G-W.) and the American Diabetes Association (J.L.).

CONFLICT OF INTEREST

None declared

APPENDIX A. SUPPLEMENTARY DATA

Supplementary data related to this article can be found at http://dx.doi.org/10.1016/j.molmet.2014.12.011.

REFERENCES

[1] Calle, E.E., Rodriguez, C., Walker-Thurmond, K., Thun, M.J., 2003. Overweight, obesity, and mortality from cancer in a prospectively studied cohort of U.S. adults. New England Journal of Medicine 348:1625–1638.

[2] Hsing, A.W., Sakoda, L.C., Chua Jr., S., 2007. Obesity, metabolic syndrome, and prostate cancer. American Journal of Clinical Nutrition 86:s843–857.

[3] Schuurman, A.G., van den Brandt, P.A., Dorant, E., Brants, H.A., Goldbohm, R.A., 1999. Association of energy and fat intake with prostate carcinoma risk: results from The Netherlands Cohort Study. Cancer 86:1019–1027.

[4] Esposito, K., Chiodini, P., Capuano, A., Bellastella, G., Maiorino, M.I., Parretta, E., et al., 2013. Effect of metabolic syndrome and its components on prostate cancer risk: meta-analysis. Journal of Endocrinological Investigation 36:132–139.

[5] Lophatananon, A., Archer, J., Easton, D., Pocock, R., Dearnaley, D., Guy, M., et al., 2010. Dietary fat and early-onset prostate cancer risk. British Journal of Nutrition 103:1375–1380.

[6] Neuhouser, M.L., Till, C., Kristal, A., Goodman, P., Hoque, A., Platz, E.A., et al., 2010. Finasteride modifies the relation between serum C-peptide and prostate cancer risk: results from the Prostate Cancer Prevention Trial. Cancer Prevention Research (Philadelphia) 3:279–289.

[7] Dann, S.G., Selvaraj, A., Thomas, G., 2007. mTOR Complex1-S6K1 signaling: at the crossroads of obesity, diabetes and cancer. Trends in Molecular Medicine 13:252–259.

[8] Menendez, J.A., Lupu, R., 2007. Fatty acid synthase and the lipogenic phenotype in cancer pathogenesis. Nature Reviews Cancer 7:763–777.

[9] Freeman, M.R., Solomon, K.R., 2011. Cholesterol and benign prostate disease. Differentiation 82:244–252.

[10] Stambolic, V., Suzuki, A., de la Pompa, J.L., Brothers, G.M., Mirtsos, C., Sasaki, T., et al., 1998. Negative regulation of PKB/Akt-dependent cell survival by the tumor suppressor PTEN. Cell 95:29–39.

[11] Weng, L.P., Smith, W.M., Brown, J.L., Eng, C., 2001. PTEN inhibits insulin-stimulated MEK/MAPK activation and cell growth by blocking IRS-1 phosphorylation and IRS-1/Grb-2/Sos complex formation in a breast cancer model. Human Molecular Genetics 10:605–616.

[12] Garcia-Cao, I., Song, M.S., Hobbs, R.M., Laurent, G., Giorgi, C., de Boer, V.C., et al., 2012. Systemic elevation of PTEN induces a tumor-suppressive metabolic state. Cell 149:49–62.

[13] Steck, P.A., Pershouse, M.A., Jasser, S.A., Yung, W.K., Lin, H., Ligon, A.H., et al., 1997. Identification of a candidate tumour suppressor gene, MMAC1, at chromosome 10q23.3 that is mutated in multiple advanced cancers. Nature Genetics 15:356–362.

[14] Phin, S., Moore, M.W., Cotter, P.D., 2013. Genomic rearrangements of in prostate cancer. Frontiers in Oncology 3:240.

[15] Leinonen, K.A., Saramaki, O.R., Furusato, B., Kimura, T., Takahashi, H., Egawa, S., et al., 2013. Loss of PTEN is associated with aggressive behavior in ERG-positive prostate cancer. Cancer Epidemiology, Biomarkers & Prevention 22:2333–2344.

[16] Shen, M.M., Abate-Shen, C., 2010. Molecular genetics of prostate cancer: new prospects for old challenges. Genes & Development 24:1967–2000.

[17] Wong, J.T., Kim, P.T., Peacock, J.W., Yau, T.Y., Mui, A.L., Chung, S.W., et al., 2007. Pten (phosphatase and tensin homologue gene) haploinsufficiency promotes insulin hypersensitivity. Diabetologia 50:395–403.

[18] Wijesekara, N., Konrad, D., Eweida, M., Jefferies, C., Liadis, N., Giacca, A., et al., 2005. Muscle-specific Pten deletion protects against insulin resistance and diabetes. Journal of Molecular Cell Biology 25:1135–1145.

[19] Stiles, B., Wang, Y., Stahl, A., Bassilian, S., Lee, W.P., Kim, Y.J., et al., 2004. Liver-specific deletion of negative regulator Pten results in fatty liver and insulin hypersensitivity [corrected]. Proceedings of the National Academy of Sciences of the United States of America 101:2082–2087.

[20] Podsypanina, K., Ellenson, L.H., Nemes, A., Gu, J., Tamura, M., Yamada, K.M., et al., 1999. Mutation of Pten/Mmac1 in mice causes neoplasia in multiple organ systems. Proceedings of the National Academy of Sciences of the United States of America 96:1563–1568.

[21] Bieberich, C.J., Fujita, K., He, W.W., Jay, G., 1996. Prostate-specific and androgen-dependent expression of a novel homeobox gene. Journal of Biological Chemistry 271:31779–31782.

[22] Thomsen, M.K., Ambroisine, L., Wynn, S., Cheah, K.S., Foster, C.S., Fisher, G., et al., 2010. SOX9 elevation in the prostate promotes proliferation and cooperates with PTEN loss to drive tumor formation. Cancer Research 70:979–987.

[23] Chakravarty, G., Rider, B., Mondal, D., 2011. Cytoplasmic compartmentalization of SOX9 abrogates the growth arrest response of breast cancer cells that can be rescued by trichostatin A treatment. Cancer Biology & Therapy 11:71–83.

[24] Cano, A., Perez-Moreno, M.A., Rodrigo, I., Locascio, A., Blanco, M.J., del Barrio, M.G., et al., 2000. The transcription factor snail controls epithelial-mesenchymal transitions by repressing E-cadherin expression. Nature Cell Biology 2:76–83.

[25] Folkman, J., 2002. Role of angiogenesis in tumor growth and metastasis. Seminars in Oncology 29:15–18.

[26] Zhong, H., Semenza, G.L., Simons, J.W., De Marzo, A.M., 2004. Up-regulation of hypoxia-inducible factor 1alpha is an early event in prostate carcinogenesis. Cancer Detection and Prevention 28:88–93.

[27] Beauchemin, N., Arabzadeh, A., 2013. Carcinoembryonic antigen-related cell adhesion molecules (CEACAMs) in cancer progression and metastasis. Cancer and Metastasis Reviews 32:643–671.

[28] Tilki, D., Irmak, S., Oliveira-Ferrer, L., Hauschild, J., Miethe, K., Atakaya, H., et al., 2006. CEA-related cell adhesion molecule-1 is involved in angiogenic switch in prostate cancer. Oncogene 25:4965–4974.

[29] Currie, E., Schulze, A., Zechner, R., Walther, T.C., Farese Jr., R.V., 2013. Cellular fatty acid metabolism and cancer. Cell Metabolism 18:153–161.

[30] Little, J.L., Kridel, S.J., 2008. Fatty acid synthase activity in tumor cells. Subcellular Biochemistry 49:169–194.
[31] Ferrara, N., LeCouter, J., Lin, R., Peale, F., 2004. EG-VEGF and Bv8: a novel family of tissue-restricted angiogenic factors. Biochimica et Biophysica Acta 1654:69–78.
[32] Najjar, S., Boisclair, Y., Nabih, Z., Philippe, N., Imai, Y., Suzuki, Y., et al., 1996. Cloning and characterization of a functional promoter of the rat pp120 gene, encoding a substrate of the insulin receptor tyrosine kinase. Journal of Biological Chemistry 271:8809–8817.
[33] Brown, M.S., Goldstein, J.L., 2008. Selective versus total insulin resistance: a pathogenic paradox. Cell Metabolism 7:95–96.
[34] Lin, D.L., Whitney, M.C., Yao, Z., Keller, E.T., 2001. Interleukin-6 induces androgen responsiveness in prostate cancer cells through up-regulation of androgen receptor expression. Clinical Cancer Research 7:1773–1781.
[35] Butler, M., McKay, R.A., Popoff, I.J., Gaarde, W.A., Witchell, D., Murray, S.F., et al., 2002. Specific inhibition of PTEN expression reverses hyperglycemia in diabetic mice. Diabetes 51:1028–1034.
[36] Majumder, P.K., Yeh, J.J., George, D.J., Febbo, P.G., Kum, J., Xue, Q., et al., 2003. Prostate intraepithelial neoplasia induced by prostate restricted Akt activation: the MPAKT model. Proceedings of the National Academy of Sciences of the United States of America 100:7841–7846.
[37] Grille, S.J., Bellacosa, A., Upson, J., Klein-Szanto, A.J., van Roy, F., Lee-Kwon, W., et al., 2003. The protein kinase Akt induces epithelial mesenchymal transition and promotes enhanced motility and invasiveness of squamous cell carcinoma lines. Cancer Research 63:2172–2178.
[38] Zalzali, H., Naudin, C., Bastide, P., Quittau-Prevostel, C., Yaghi, C., Poulat, F., et al., 2008. CEACAM1, a SOX9 direct transcriptional target identified in the colon epithelium. Oncogene 27:7131–7138.
[39] Phan, D., Sui, X., Chen, D.T., Najjar, S.M., Jenster, G., Lin, S.H., 2001. Androgen regulation of the cell-cell adhesion molecule-1 (Ceacam1) gene. Molecular and Cellular Endocrinology 184:115–123.
[40] Liu, J., Di, G., Wu, C.T., Hu, X., Duan, H., 2013. CEACAM1 inhibits cell-matrix adhesion and promotes cell migration through regulating the expression of N-cadherin. Biochemical and Biophysical Research Communications 430:598–603.
[41] Holash, J., Maisonpierre, P.C., Compton, D., Boland, P., Alexander, C.R., Zagzag, D., et al., 1999. Vessel cooption, regression, and growth in tumors mediated by angiopoietins and VEGF. Science 284:1994–1998.
[42] Gerstel, D., Wegwitz, F., Jannasch, K., Ludewig, P., Scheike, K., Alves, F., et al., 2011. CEACAM1 creates a pro-angiogenic tumor microenvironment that supports tumor vessel maturation. Oncogene 30:4275–4288.
[43] Najjar, S.M., Russo, L., 2014. CEACAM1 loss links inflammation to insulin resistance in obesity and non-alcoholic steatohepatitis (NASH). Seminars in Immunopathology 36:55–71.
[44] Park, E.J., Lee, J.H., Yu, G.Y., He, G., Ali, S.R., Holzer, R.G., et al., 2010. Dietary and genetic obesity promote liver inflammation and tumorigenesis by enhancing IL-6 and TNF expression. Cell 140:197–208.
[45] Ying, H., Elpek, K.G., Vinjamoori, A., Zimmerman, S.M., Chu, G.C., Yan, H., et al., 2011. PTEN is a major tumor suppressor in pancreatic ductal adenocarcinoma and regulates an NF-kappaB-cytokine network. Cancer Discovery 1:158–169.
[46] Smith, D.A., Kiba, A., Zong, Y., Witte, O.N., 2013. Interleukin-6 and oncostatin-M synergize with the PI3K/AKT pathway to promote aggressive prostate malignancy in mouse and human tissues. Molecular Cancer Research 11:1159–1165.
[47] Flammiger, A., Weisbach, L., Huland, H., Tennstedt, P., Simon, R., Minner, S., et al., 2013. High tissue density of FOXP3+ T cells is associated with clinical outcome in prostate cancer. European Journal of Cancer 49:1273–1279.
[48] Bandyopadhyay, S., Pai, S.K., Watabe, M., Gross, S.C., Hirota, S., Hosobe, S., et al., 2005. FAS expression inversely correlates with PTEN level in prostate cancer and a PI 3-kinase inhibitor synergizes with FAS siRNA to induce apoptosis. Oncogene 24:5389–5395.
[49] Migita, T., Ruiz, S., Fornari, A., Fiorentino, M., Priolo, C., Zadra, G., et al., 2009. Fatty acid synthase: a metabolic enzyme and candidate oncogene in prostate cancer. Journal of the National Cancer Institute 101:519–532.
[50] Bigorgne, A.E., Bouchet-Delbos, L., Naveau, S., Dagher, I., Prevot, S., Durand-Gasselin, I., et al., 2008. Obesity-induced lymphocyte hyperresponsiveness to chemokines: a new mechanism of fatty liver inflammation in obese mice. Gastroenterology 134:1459–1469.
[51] Flavin, R., Zadra, G., Loda, M., 2011. Metabolic alterations and targeted therapies in prostate cancer. Journal of Pathology 223:283–294.
[52] Yue, S., Li, J., Lee, S.-Y., Lee, H.J., Shao, T., Song, B., et al., 2014. Cholesteryl ester accumulation induced by PTEN loss and PI3K/AKT activation underlies human prostate cancer aggressiveness. Cell Metabolism 19:393–406.
[53] Ittmann, M., Huang, J., Radaelli, E., Martin, P., Signoretti, S., Sullivan, R., et al., 2013. Animal models of human prostate cancer: the consensus report of the New York meeting of the mouse models of Human Cancers Consortium Prostate Pathology Committee. Cancer Research 73:2718–2736.

